Journal of Molecular Liquids 263 (2018) 1–9

Contents lists available at ScienceDirect

Journal of Molecular Liquids

journal homepage: www.elsevier.com/locate/molliq

Cosolubilization of phenanthrene and pyrene in surfactant micelles: Experimental and atomistic simulations studies

Xujun Liang [a,c], Chuling Guo [a,b,*], Shasha Liu [a], Zhi Dang [a,b], Yanfu Wei [d], Xiaoyun Yi [a,b], Stéphane Abel [e,**]

[a] School of Environment and Energy, South China University of Technology, Guangzhou 510006, China
[b] The Key Lab of Pollution Control and Ecosystem Restoration in Industry Clusters, Ministry of Education, Guangzhou 510006, China
[c] School of Environment, Guangzhou Key Laboratory of Environmental Exposure and Health, and Guangdong Key Laboratory of Environmental Pollution and Health, Jinan University, Guangzhou 510632, China
[d] CAS Key Laboratory of Mineralogy and Metallogeny/Guangdong Provincial Key Laboratory of Mineral Physics and Materials, Guangzhou Institute of Geochemistry, Chinese Academy of Sciences, Guangzhou 510640, China
[e] Institut de Biologie Inté grative de la Cellule (I2BC), Institut Frédéric Joliot, CEA, CNRS, Univ Paris-Sud Université Paris-Saclay, 91405 Gif-Sur-Yvette Cedex, France

ARTICLE INFO

Article history:
Received 8 September 2017
Received in revised form 6 March 2018
Accepted 24 April 2018
Available online 26 April 2018

Keywords:
Surfactant
Phenanthrene
Pyrene
Cosolubilization
Molecular dynamics simulations

ABSTRACT

Solubilization of mixed phenanthrene (PHE) and pyrene (PYR) in Triton X-100 (TX), sodium dodecyl sulfate (SDS) and mixed TX-SDS surfactant solutions were done to observe their cosolubilization effect. Moreover, molecular dynamics (MD) simulations were performed to reveal how polycyclic aromatic hydrocarbons (PAHs) coexist in the micelle. Cosolubilization of PHE and PYR exhibited synergism along with decreasing synergistic extent with increasing SDS in mixed micelle. MD simulations verified the distribution of PHE and PYR in the shell and core regions of pure SDS and mixed SDS-TX micelles (with molar ratio of 1: 1), which were chosen as the representative systems for simulation study. The movement of PHE and PYR inside the micelle along with their different probability to contact with SDS non hydrogen atoms in pure SDS and mixed SDS-TX solubilization systems suggests the different solubilization sites of the two PAHs inside the micelle leading to their coexistence in the micelle. This study implies the significance of considering cosolubilization effects between PAH mixtures in determining surfactant concentration for environmental remediation.

© 2018 Elsevier B.V. All rights reserved.

1. Introduction

With increasing industrialization and urbanization around the world, there is an increasing demand and consumption of fossil fuels. Incomplete combustion or pyrolysis of the fossil fuels has produced a group of ubiquitous organic contaminants such as polycyclic aromatic hydrocarbons (PAHs) [1,2]. PAHs are a global environmental concern due to their carcinogenic, teratogenic and mutagenic effects on both human and ecosystem [3,4]. Due to their hydrophobicity, PAHs incline to deposit into soil [5]. Surfactant-enhanced remediation (SER) has been studied and assessed as an efficient technology for the decontamination of PAHs from soil [6–9]. Surfactants' solubilization power towards PAHs is one of the main drivers governing SER efficiency. Most studies focused on observing solubilization of individual PAHs into single, binary or ternary surfactant systems [10–15]. However, PAHs exist in complex mixtures in contaminated sites. Previous reports have shown that cosolubilization of mixed organic pollutants in surfactant micelles exhibits inconsistent effects - synergistic, inhibitive or little impact on each other's solubility [16–20]. At present, researches concerning cosolubilization of mixed low-molecular-weight (LMW, molecules formed by 2- and 3- benzene rings) and high-molecular-weight (HMW, molecules composed of ≥4 benzene rings) PAHs in single and binary surfactant systems are limited.

Cosolubilization effect between mixed PAHs has been related to the solubilization sites of PAHs inside surfactant micelles. Rouse et al. found that, fluorene and phenanthrene (PHE) could compete for a similar locus in the micelle due to their resemble hydrophobicity, thus contributing to their decreasing solubility when coexisted in surfactant solutions [18]. Yang et al. also found that solubilization of naphthalene (NAP) and pyrene (PYR) in micelle shell could reduce micelle-water interfacial tension and increase micelle internal volume to solubilize more NAP and PYR with different solubilization sites [19]. The locus of PAHs inside the micelle can be detected by various experimental techniques such as NMR [21], UV–visible [22] and fluorescence [23] spectroscopy. However, due to the small size of the micelle and the existence of solvents, it is difficult to attain a clear and microscopic view of the distribution of PAHs inside the micelle using the experimental approaches. By using molecular dynamics (MD) simulation approaches, Liang et al. observed that NAP and PYR could dynamically partition in the shell and

* Correspondence to: C. Guo, School of Environment and Energy, South China University of Technology, Guangzhou 510006, China.
** Corresponding author.
E-mail addresses: clguo@scut.edu.cn (C. Guo), stephane.abel@cea.fr (S. Abel).

https://doi.org/10.1016/j.molliq.2018.04.123
0167-7322/© 2018 Elsevier B.V. All rights reserved.

core regions of a micelle formed by 60 sodium dodecyl sulfate (SDS) monomers due to the movement of the two PAHs inside the micelle [24]. Although the distribution of single PAHs inside the micelle has been revealed, how mixed PAHs coexist inside the micelle remains unclear.

Herein, in this study, the solubilization and cosolubilization of mixed LMW and HMW PAHs in pure SDS, Triton X-100 (TX) and their mixed surfactant solutions was firstly investigated. Then pure SDS micelle and mixed SDS-TX micelle (with molar ratio of 1: 1) were selected as representative systems for performing MD simulations of cosolubilization of PAH mixtures to observe the potential mechanisms controlling their coexistence in the micelle. PHE and PYR were chosen as model LMW and HMW PAHs, respectively, due to their wide distribution in urban and coking plant soil [25,26]. This study will further our understanding of cosolubilization mechanisms of PAH mixtures in surfactant micelles.

2. Materials and methods

2.1. Chemicals

PHE and PYR with purities > 98% were purchased from Sigma Aldrich Chemical Company. TX (purity ≥ 99%) and SDS (purity 98%) were chosen as the model nonionic and anionic surfactants, respectively, since they were widely used in industry and subsurface remediation [27,28]. The two surfactants were also obtained from Sigma Aldrich Chemical Company. Physicochemical properties of PHE, PYR, TX and SDS were listed in Fig. 1. Deionized water was used for preparing surfactant solutions. HPLC-grade methanol (Shanghai Anpel Scientific Instrument Co., Ltd) was used for standard solution preparation and sample dilution.

2.2. Solubilization experiments

Solubilization experiments were done according to the previous report [17]. Briefly, an excess amount of solid PHE and PYR with single or binary combinations were weighted to 30 mL borosilicate vials. Then, 20 mL of surfactant solutions with TX/SDS molar ratio of 5/0, 4/1, 1/1, 2/3 and 0/5 were added to each vial. Surfactant concentrations for pure SDS solubilization systems were set as 10, 20, 30, 40 and 50 mM, whereas the other solubilization systems were 2, 4, 6, 8 and 10 mM. The surfactant concentrations set were all above their CMC [17]. Afterwards, the vials were equilibrated on a reciprocating shaker for 48 h at 150 rpm and 25 °C. Then, the vials were centrifuged at 4000 rpm for 1 h to separate the solid and aqueous phases, and an adequate volume of the supernatant was taken and diluted with methanol for HPLC analysis. Standard solutions were prepared by dissolving mixed PHE and PYR in methanol and stored at 4 °C for further use.

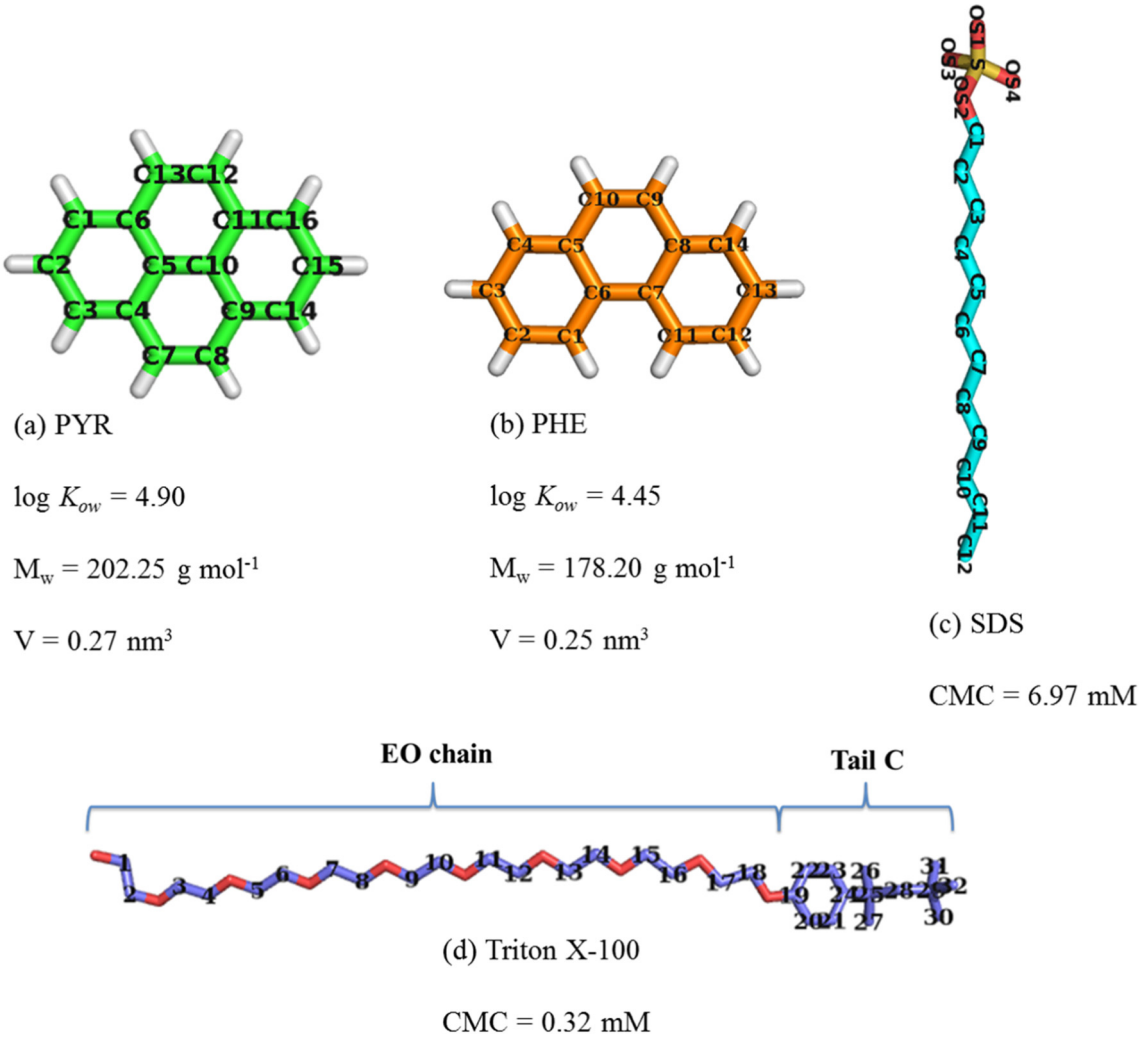

Fig. 1. Physicochemical properties and carbon numbers of (a) pyrene (PYR), (b) phenanthrene (PHE), (c) SDS, and (d) Triton X-100 (TX). The proton atoms of SDS and TX are removed for clarity in numbering the carbon atoms. The physicochemical properties of PHE and PYR are cited from *Ref.* [29]. V means the molecular Voronoi volume of PHE/PYR in our simulations, which is computed with the *trjVoronoi* program [30,31]. CMC means the critical micelle concentration of SDS and Triton X-100, which were cited from *Ref.* [17].

2.3. Analytical methods

The samples were analyzed on an Agilent 1200 HPLC equipped with a diode array detector and an Agilent Eclipse XDB-C18 column (5 μm, 4.6 × 150 mm). The mobile phase was 70/30 (v/v) methanol/water. The flow rate was set at 1.0 mL min^{-1}. The detection wavelength was set at 234 nm for PYR and 250 nm for PHE. Surfactants in the samples were low enough to avoid interference during PAHs detection.

2.4. Molecular dynamics simulations of mixed PHE and PYR in pure SDS and mixed SDS-TX micelle

Three MD simulation systems were done to compare the cosolubilization characteristics of PAH mixtures in different micelle systems. System I as pure SDS micelle solubilization system was composed of 60 SDS, 8 PHE and 5 PYR molecules. System II as mixed SDS-TX micelle system was formed by 32 SDS and 31 TX molecules to represent an SDS/TX molar ratio of 1/1. The components of System III were similar to System II except the addition of 10 PHE and 7 PYR molecules to simulate mixed micelle solubilization system. The aggregation number of pure SDS and mixed SDS-TX micelle with molar ratio of 1/1 was set according to previous fluorescence quenching experiments [32,33] and MD simulations [34,35]. The numbers of PHE and PYR added in the solubilization simulation systems were estimated from our enhanced solubilization experiments. All the molecules in this study were modeled with the CHARMM force field. In the case of SDS and TX surfactants, the parameters available in the CHARMM distribution [36,37] and described in Yordanova et al. [38] were used, respectively. For PHE and PYR, the bonded and non-bonded parameters were based on the CHARMM general FF (CGenFF) [39,40].

All MD simulations were performed using the GROMACS 5.0.4 package [41,42]. Simulation details were given in our previous study with slight modifications [24]. In brief, the surfactant monomers in each simulation system were preassembled as a spherical aggregate using Packmol [43]. The prepacked micelle was then inserted into a cubic box of ~10 nm on each side, with PHE and PYR introduced randomly around the micelle surface. Water was modeled with the CHARMM TIP3P model [44]. Sodium ions were added to neutralize the system. Then, the constructed system was energy minimized with the steepest descent algorithm (<1000.0 kJ/ mol nm^{-1}). Afterwards, the NVT ($T = 300$ K) and NPT ($T = 300$ K and $P = 1.015$ bars) ensembles were used to equilibrate the system for 400 ps and 1 ns, respectively. During NVT and NPT, the temperature and pressure were controlled by the v-rescale [45] thermostat ($\tau_T = 0.1$ ps) and Berendsen [46] barostat ($\tau_P = 2.0$ ps). During these periods the SDS and TX molecules were allowed to relax, whereas the PAHs were kept fixed. Finally, the production runs were carried out at $T = 300$ K and $P = 1.015$ bars with the temperature and pressure controlled by the v-rescale thermostat [45] ($\tau_T = 0.1$ ps) and the Parrinello-Rahman [47,48] barostat (($\tau_P = 3.0$ ps). Periodic boundary conditions were used with a time step of 2 fs for integrating the equation of motions. The Particle Mesh Ewald method [49] was used to compute the long range electrostatic interactions with a cutoff of 1.2 nm. The Lennard-Jones interactions were treated with a switch potential with $r_{vdw\text{-}switch} = 1.0$ nm and $r_{vdw} = 1.2$ nm.

To estimate the length of production time for each simulation system, the radius of gyration R_g, of the micelle or micelle-PAH complex as a function of time was computed. As shown in Fig. S1, R_g of the SDS micelle-PAH complex in System I reached stable at around 1.65 nm after ~124 ns, meaning that all PAH molecules have partitioned into the SDS micelle. To have enough sampling for analyzing simulation results, the production runs were then continued for another 80 ns after all PAHs partitioned into the micelle in System I. As for Systems II and III, R_g of mixed SDS-TX micelle or mixed micelle-PAH complex was stable at ~2.00 nm during the simulation time (Fig. S2). The micelle size of the pure SDS and mixed SDS-TX micelle are close to the previous reports [32,34,50].

It is difficult to differentiate the time when all PAH molecules enter into the micelle in System III. Therefore the instantaneous distance between the center of mass (COM) of PHE/PYR and mixed micelle in System III was calculated. As shown in Fig. S3, the COM distance between PHE/PYR and micelle kept within ~2.60 nm after 20 ns in System III, indicating that all PAH molecules have entered into the mixed micelle. Due to the slightly larger size of mixed SDS-TX micelle than pure SDS micelle, a production run of ~120 ns was done to ensure enough samplings for analysis. The trajectories were analyzed by GROMACs tools and *home-made* programs.

3. Results and discussion

3.1. Solubilization and cosolubilization of PHE and PYR in different surfactant systems

Surfactants' solubilization potential towards PHE and PYR was characterized by the molar solubilization ratio (MSR) and the micelle-water partition coefficient, K_m. MSR is defined as the number of moles of compounds solubilized per mole of surfactant micelle, which can be computed directly from the slope of linear fitting of the solubilization curve [51]. Detailed methods to compute K_m for single and mixed PAH solubilization systems are described in the Supporting Information. Furthermore, to quantify the cosolubilization effects, the deviation ratio $R_{\Delta MSR}$ is defined [17,19]:

$$R_{\Delta MSR}\% = \frac{MSR_{binary} - MSR_{single}}{MSR_{single}} \times 100\% \quad (1)$$

where, MSR_{single} and MSR_{binary} are MSR values of a given solute in a single solubilization and a binary cosolubilization system, respectively.

The MSR, K_m and $|R_{\Delta MSR}|$ of PHE and PYR in their single and binary mixed state in different solubilization systems are listed in Tables 1 and 2.

In single PHE solubilization system, the MSR of PHE in pure SDS solutions was 0.032, in accordance with the reported values, 0.031 [17,52]. In single PYR solubilization system, the MSR of PYR in pure SDS solutions was 0.010, the same as the reported value, 0.010 [53]. Moreover, the MSRs of PHE and PYR increase with increasing TX in the micelle. In all solubilization systems, PHE had lower K_m values than PYR, indicating that PYR had stronger affinity to the micelle due to the larger log K_{ow} value of PYR.

As shown in Fig. 2 and Table 1, cosolubilization of PHE and PYR in mixed TX-SDS (mole ratio, 4:1) surfactant systems exhibited synergistic effect, namely solubility of PHE and PYR was both increased when added simultaneously in surfactant solutions. Synergism between PHE and PYR was also occurred in other surfactant systems (Figs. S4–S7). Furthermore, the synergistic extent between PHE and PYR decreased with increasing percentage of SDS in the mixed micelle, reaching the

Table 1
Molar solubilization ratio (MSR) and micelle-water partition coefficient K_m of phenanthrene (PHE) and pyrene (PYR) in the solubilization systems.

TX/SDS	PHE		PYR	
	MSR/K_m (10^5)[a]		MSR/K_m (10^6)[a]	
	PHE	PHE-PYR	PYR	PYR-PHE
5/0[b]	0.13/9.66	0.15/10.47	0.044/6.14	0.052/6.32
4/1	0.086/6.65	0.095/7.02	0.036/5.07	0.040/5.14
1/1	0.058/4.60	0.062/4.78	0.023/3.28	0.026/3.48
2/3	0.053/4.22	0.055/4.29	0.020/2.86	0.021/2.85
0/5	0.032/2.60	0.032/2.58	0.010/1.44	0.010/1.40

[a] Error limits of MSR and *K*m are within 2%.
[b] Values taken from Ref. [40].

Table 2
$R_{\Delta MSR}$, $\Delta G^{\circ}_{excess}$ and ω/RT between binary mixtures of phenanthrene (PHE) and pyrene (PYR) at 25 °C in different surfactant systems.

TX/SDS	$\lvert R_{\Delta MSR}\rvert$ (%)		$\Delta G^{\circ}_{excess}$ (kJ/mol)	ω/RT
	PHE	PYR		
5/0	15.38	18.19	−3.02	−6.33
4/1	10.46	11.11	−2.40	−4.62
1/1	6.90	13.04	−1.45	−2.79
2/3	3.77	5.00	−0.89	−1.78
0/5	0	0	0.90	2.00

Error limits of $R_{\Delta MSR}$, $\Delta G^{\circ}_{excess}$ and ω/RT are ±2%.

minimum in pure SDS solutions. The synergism was furtehr quantified by the deviation ratio $|R_{\Delta MSR}|$. As indicated in Table 2, $|R_{\Delta MSR}|$ generally decreases with increasing SDS in mixed micelle. Cosolubilization synergism between PAHs with different log K_{ow} values was observed in previous studies [16,21]. They presumed that PAHs solubilized in micelle shell could reduce the micelle-water interfacial tension thus increasing the micelle internal volume to solubilize more PAHs with different solubilization sites inside the micelle. Therefore, synergism between PHE and PYR is assumed to be: i) PHE and PYR can reside in both shell and core regions of the micelle according to the ^{1}H chemical shifts data in previous reports [17,19]; ii) PHE and PYR may have different solubilization sites owing to their different hydrophobicity (Fig. 1); iii) PAHs solubilized in the shell region are able to decrease the interfacial tension, enabling the micelle volume to increase cooperatively to some extent for solubilizing more solutes [54]; and iv) PYR has stronger affinity to the micelle than PHE due to its larger K_{ow} (Fig. 1), leading to its stronger solubility enhancement. The decreasing synergistic extent with increasing SDS is due to the decrease of micelle size with increasing SDS in the micelle.

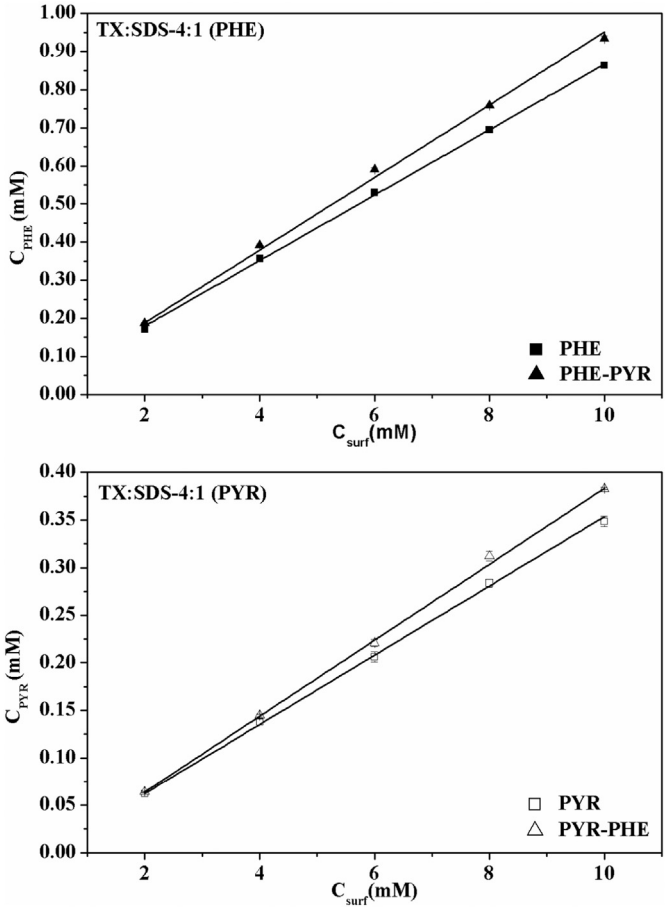

Fig. 2. Enhanced solubility of phenanthrene (PHE) and pyrene (PYR) as individual compounds and their respective dual mixtures in TX/SDS (4/1) mixed surfactant systems. Symbols represent experimental values, and lines represent linear regression. The error bars stand for the standard deviation of the triplicate samples at each concentration and are, in most cases, smaller than the symbols.

Two thermodynamical parameters, excess Gibbs energy '$\Delta G^{\circ}_{excess}$' and interaction parameter 'ω/RT', introduced by Nagadome et al. [55] and Masrat et al. [56], were used to further interpret the miscibility between PHE and PYR in the micelle. The excess Gibbs energy '$\Delta G^{\circ}_{excess}$' and interaction parameter "ω" can be computed as described below [17].

The solubilization equilibria when PAHs are used in excess can be expressed as follows:

$$\text{Solid PAH(crystal)} \overset{K_d}{\rightleftharpoons} \text{Singly dispersed PAH in bulk} \overset{K_m}{\rightleftharpoons} \text{Solubilized PAH in micelles}$$
$$\Delta G^{\circ}_{d} = -RT \ \ln K_d \qquad\qquad \Delta G^{\circ}_{m} = -RT \ \ln K_m$$

where K_d is taken equal to its water solubility, S_{CMC}. The equilibrium constant of solubilization corresponding to the translation from the solid state to the solubilized state in micelles is, therefore, given by

$$K_{eq} = K_d \times K_m \tag{2}$$

herein K_m is the partition coefficient of PAHs between aqueous phase and micellar phase. Values of K_m were calculated from Eq. (S1) in the Supporting Information for single solubilization system. For cosolubilization of two solid solutes, A and B, the total equilibrium constant of cosolubilization will be calculated by

$$K^{mix}_{eq} = \left(K^{A}_{d} \times K^{A}_{m}\right) \times \left(K^{B}_{d} \times K^{B}_{m}\right) \tag{3}$$

where K^{A}_{m} and K^{B}_{m} are their respective partition coefficients in mixed solubilization systems and can be computed by Eq. (S2). Consequently, the Gibbs free energy change of single solubilizate system and two solubilizates system will be represented as follows:

$$\Delta G^{\circ} = -\text{RT} \ \ln K_{eq} \tag{4}$$

$$\Delta G^{\circ}_{mix} = -\text{RT} \ \ln K^{mix}_{eq} \tag{5}$$

If the mixture is ideally formed, the molar Gibbs energy of ideal mixing ΔG°_{mix}(ideal) should satisfy the additive rule as

$$\Delta G^{\circ}_{mix}(\text{ideal}) = X^{A}\Delta G^{\circ}_{A} + X^{B}\Delta G^{\circ}_{B} \tag{6}$$

X^A and X^B are the mole fractions of the two species 'A' and 'B' within the micelles on the solubilizate only basis and were computed as

$$X^{A} = \frac{MSR_A}{MSR_A + MSR_B} \tag{7}$$

The difference between the real value of the free energy change ΔG°_{mix} and ΔG°_{mix}(ideal) gives the excess Gibbs energy

$$\Delta G^{\circ}_{excess} = \Delta G^{\circ}_{mix} - \left(X^{A}\Delta G^{\circ}_{A} + X^{B}\Delta G^{\circ}_{B}\right) \tag{8}$$

The interaction parameter 'ω', signifying the cohesive forces between the unlike solubilizates are calculated based on the excess Gibbs energy and expressed as the following equation:

$$\omega = \frac{\Delta G^{\circ}_{excess}}{\left(X^{A}X^{B}\right)} \tag{9}$$

The negative values of 'ω/RT' obtained mean that the interaction between two solutes was enhanced, and two solutes are more miscible with lower 'ω/RT' values [55,56]. Computed $\Delta G^{\circ}_{excess}$ and ω/RT are listed in Table 2. The computed $\Delta G^{\circ}_{excess}$ and ω/RT increase with increasing

mole ratio of SDS in the mixed micelle, meaning that the miscibility between PHE and PYR becomes weaker with increasing SDS. This verifies that the decreasing micelle size with increasing SDS is sterically unfavorable for solubilizing PAHs, contributing to the decreasing synergistic extent.

Although NMR chemical shifts show that PHE and PYR could distribute in both the shell and core regions of the micelle, whether they have different solubilization sites inside the micelle is difficult to be directly revealed by the experimental approaches. Hence, in the following sections, the MD results describing solubilization of mixed PHE and PYR in pure SDS and mixed SDS-TX micelle will be presented to provide a direct view of how PAHs coexist inside the micelle.

3.2. Distribution and movements of mixed PHE and PYR in different micelles

3.2.1. Distribution of mixed PHE and PYR in the micelle

To observe the locus of PHE and PYR in the SDS and mixed SDS-TX micelle, the radial density profiles (RDPs) of corresponding SDS subunits (i.e. headgroup, C1, C6 and C12), TX subunits (.i.e. ethylene oxide (EO) chain and tail carbon atoms) and the center of mass (COM) of PHE/PYR with respect to the micelle COM were computed (Fig. 3).

As shown in Fig. 3a the RDP of the SDS headgroup exhibits a strong peak at about 2.0 nm from the micelle COM corresponding approximately to the micelle size represented by the R_g values given in the Section 2.4. Water RDP has a wide overlap with the RDPs of SDS headgroup, C1 and C6 atoms, which means that water could not only solvate the SDS headgroup, but also penetrate to a limited extent into the micelle hydrophobic region. The RDP of the SDS C1 atom shows maxima at around 1.8 nm indicating its main locus in the micelle surface. C6 mainly located at distance about 1.2 nm from the micelle COM. C12 shows wide RDP meaning that C12 can distribution in both micelle core and shell regions. The computed RDPs of SDS subunits in the mixed PAH solubilization system is similar to that for pure SDS micelle observed in the previous work [24], which means that solubilization of PHE and PYR inside the micelle has little impact on micelle internal structure. In terms of PHE and PYR, both of them obtains peak RDPs at around 1.5 nm and near micelle core, meaning that they can distribute in the micelle shell and core regions simultaneously when coexisted in the micelle. This is in line with our experimental studies. Yang et al. [19] observed that the ^{1}H chemical shift of all hydrogen atoms belonging to sodium dodecyl benzene sulfonate (SDBS) was significantly changed by the solubilization of PYR, indicating the presence of PYR in both the micelle shell and core regions of SDBS. Furthermore, changes of the SDS ^{1}H chemical shifts were observed after the solubilization of PHE inside the micelle [17].

Fig. 3b shows that in the mixed SDS-TX simulation system (System II), water RDP has a wide overlap with the RDPs of SDS headgroup, C1 and C6 atoms, TX tail carbon atoms and TX EO chains. The RDP of SDS headgroup ranges from 1.2 to 3.2 nm with a peak at ~1.8 nm. The RDPs of the SDS C1 and C6 atoms shows maxima at ~1.6 nm and 1.0 nm from the micelle COM. Both SDS C12 and TX carbon atoms show wide RDP meaning that they can distribute in both micelle core and shell regions. The RDP of TX EO chain covers a wide range (0.4–3.8 nm) along with a peak at ~1.8 nm. The wider RDP of TX EO chain than SDS headgroup implies the incorporation of SDS molecules into TX aggregates in the mixed SDS-TX micelle system, which is in accordance with that described by Wang et al. [57], who reported the insertion of SDS into TX micelles through 2D NOESY NMR investigations. In terms of PHE and PYR, both of them obtains wide RDPs from micelle core to micelle surface, implying their simultaneous distribution in the micelle shell and core regions when coexisted in mixed SDS-TX micelle. Interestingly, unlike pure SDS micelle solubilization system (System I), the solubilized PHE and PYR molecules could expel SDS and TX molecules away from micelle core, causing the slight shift of the RDPs of SDS and TX subunits from micelle center. This may make PHE and PYR easier to stay in the core of mixed SDS-TX micelle than pure SDS micelle, as verified by the higher percentage of simulation time for PHE/PYR to stay in micelle core in System III than System I (Section 3.2).

Though the RDPs of PHE and PYR verify the partition of the two PAHs in both the shell and core regions of the micelle, it is difficult to reveal the preferred locus of PAHs in mixed PAH solubilization systems, especially along the surfactant alkyl chains. Hence, the probability distribution that a given SDS heavy atom or TX backbone carbon atoms is

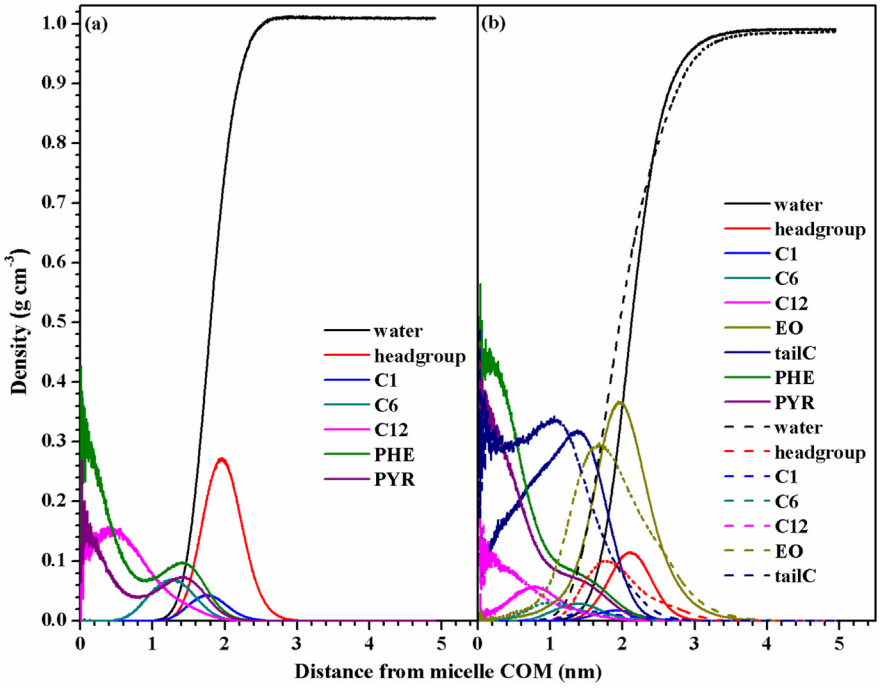

Fig. 3. Radial density profiles of SDS subunits, TX subunits, phenanthrene (PHE) and pyrene (PYR) with respect to the micelle center of mass in (a) System I and (b) Systems II and III. Headgroup, C1, C6, and C12 represent the subunits belonging to the SDS molecule, as depicted in Fig. 1c. EO and tailC represent the subunits of TX molecule, as illustrated in Fig. 1d. Panel (b): results computed from Systems II (dashed line) and III (solid line).

closest to the C5 atoms of PYR and C6 atoms of PHE is computed. The probability distributions were determined by first calculating the minimum distances between any SDS heavy atom/TX backbone carbon atom and the PYR C5 or PHE C6 atoms. Then, a tally of the closest heavy atom in the SDS or TX molecule and the C5 or C6 atoms in the PAH molecules were kept. This information was then normalized.

As shown in Fig. 4a, both the C5 atoms of PYR and the C6 atoms of PHE have no contact with the sulfur atoms of SDS in Systems I and III due to the steric and electrostatic energy barriers stemming from the three oxygen atoms surrounding the sulfur [58]. Furthermore, PHE and PYR exhibit different probability to contact with different SDS heavy atoms in Systems I and III. Specifically, in mixed PAH systems, the order of the probability of the two PAHs to contact with the oxygen, front and terminal carbon atoms of SDS follows: PHE > PYR, whereas the probability to contact with the middle carbon atoms (i.e. C5-C10) follows: PYR > PHE. However, it is shown that PHE and PYR have similar probability to contact with TX backbone carbon atoms (Fig. 4b).

To further illustrate the different trends of PAH molecules to contact with SDS alkyl and TX backbone chains, the internal dynamics of SDS alkyl/TX carbon atoms and C5 atoms of PYR and the C6 atoms of PHE were examined by computing their amplitude of displacements (ADs).

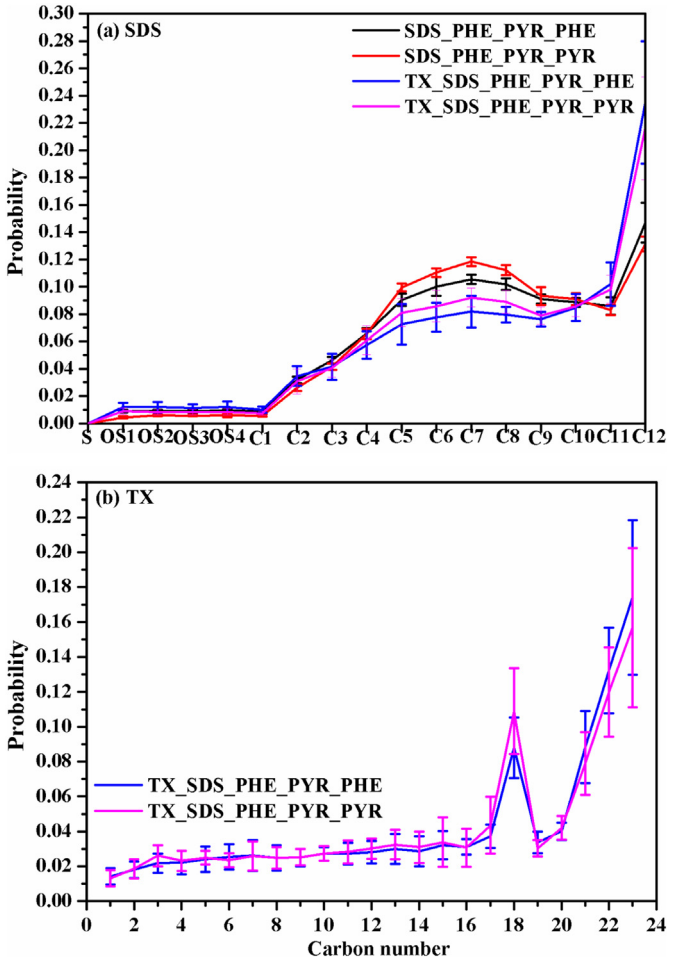

Fig. 4. Normalized probability distribution of C5 atoms of pyrene (PYR) and C6 of phenanthrene (PHE) to contact with (a) SDS heavy atoms and (b) TX backbone carbon atoms. The C5 atoms of pyrene (PYR) and C6 of phenanthrene (PHE) are adjacent to the center of mass of the two PAH molecules, as depicted in Fig. 1. The C20, C21, C22 and C23 in Panel (b) mean C24, C25, C28 and C29 atoms of TX (Fig. 1d). The black and red lines in Panel (a) mean the probability of PHE and PYR to contact with SDS heavy atoms in System I. The blue and magenta lines in Panels (a)–(b) represent the probability of PHE and PYR to contact with SDS heavy atoms and TX main carbon atoms in System III, respectively.

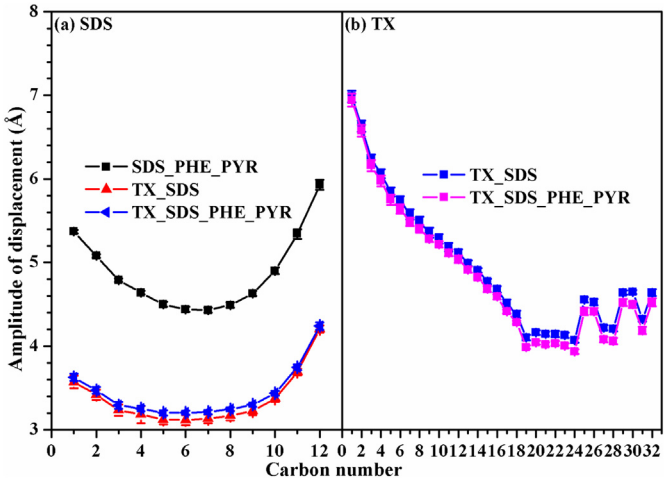

Fig. 5. Variations of the amplitude of displacement (AD) of (a) SDS carbon atoms and (b) TX carbon atoms in Systems I–III. The carbon numbers correspond to their positions along the SDS and TX chain, as shown in Fig. 1.

The ADs were calculated according to the method described by Aoun et al. [59]. As presented in Fig. 5, in the mixed micelle solubilization system (System III), the ADs of TX carbon atoms are in the range of 4–7 Å, which are larger than that of the SDS carbon atoms (3–4.2 Å) and PHE C6 atom (3.21 ± 0.04 Å) and PYR C5 atom (3.05 ± 0.05 Å). The larger ADs of TX carbon atoms may facilitate their contact with PHE and PYR molecules contributing to the similar probability of PHE and PYR to contact with TX backbone carbon atoms. Furthermore, the ADs of SDS carbon atoms (4.5–6 Å), PHE C6 atom (4.97 ± 0.10 Å), and PYR C5 atom (4.90 ± 0.11 Å) in System I are greater than that observed in System III. This further verifies the incorporation of SDS molecules into the aggregate formed by TX molecules in the mixed micelle solubilization system. Since PHE and PYR have similar ADs as SDS molecules in both pure SDS solubilization system (System I) and mixed SDS-TX solubilization system (System III), the different probability of the two PAHs to contact with the SDS heavy atoms indicates their different solubilization sites inside the micelle to coexist inside the micelle. Moreover, solubilization of PAHs in the mixed SDS-TX micelle has little impact on micelle internal dynamics (Fig. 5). The ADs of SDS alkyl carbon atoms computed from System I are similar to the ADs for pure SDS micelle as computed in the previous study [24].

3.2.2. Movements of PAHs in SDS and mixed SDS-TX micelle

In our previous work, NAP and PYR were found to exchange frequently between micelle shell and core region during the simulation time [24]. Movement of PHE and PYR in the mixed PAH solubilization system was also observed. As shown in Fig. 6 under mixed PHE/PYR condition, the marked PHE/PYR located in the core region can move towards the micelle surface, as do the other PHE/PYR molecules, and vice versa. Through measuring the fluorescence lifetime of 2-ethylnaphthalene (2EN) in several cationic micelles such as dodecyl trimethylammonium chloride, Cang et al. [60] found that 2EN could exchange between the shell and core regions of the micelle on a nanosecond time scale.

To quantify the duration of PHE and PYR to stay in micelle shell and core regions, the time percentage of the two PAHs to stay in each region of the micelle was computed. As shown in Table 3, PHE and PYR spend relatively high percentage of simulation time to stay in the micelle shell (75–79% in System I within 80 ns production time and 63–67% in System III within 120 ns production time), suggesting their preference to stay in micelle shell. Yet in the mixed micelle solubilization system, it is interesting that PHE and PYR exhibited higher percentage of time to stay in the core region than in pure SDS micelle (System I). This may be attributed to the possibility of PHE/PYR to slightly expel SDS and

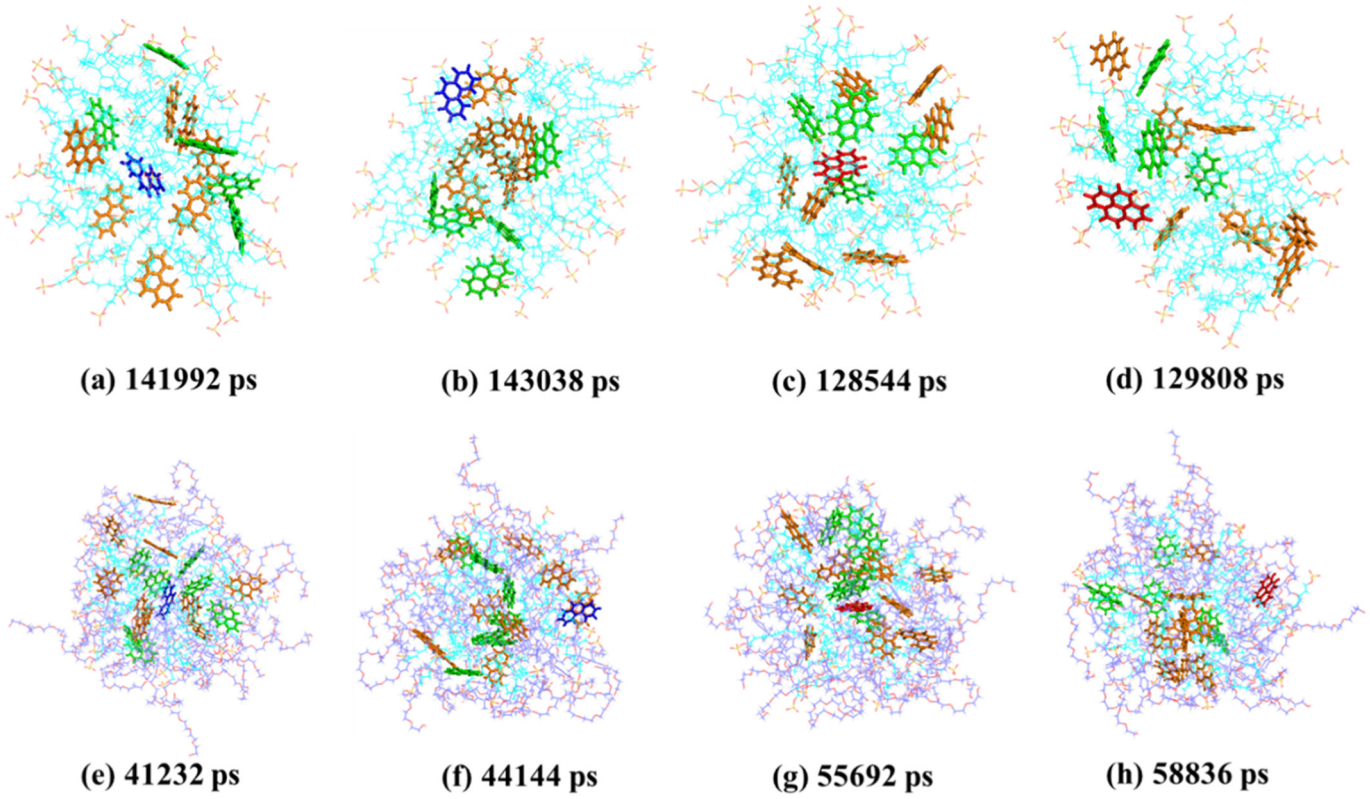

Fig. 6. Representative snapshots showing the movement of phenanthrene (PHE) and pyrene (PYR) in the micelle extracted from Systems I (a–d) and III (e–f). PHE is denoted by orange, except one that is marked as blue to show its translation from micelle core to surface. PYR is denoted by green, except one that is marked as red to show its translation from micelle core to surface.

TX from micelle core (Fig. 3) enabling more core volume for solubilizing PHE/PYR. The probability distribution of the distance between PAH and micelle COM, as well, indicates that PHE/PYR exist higher probability to stay in the shell (Fig. 7). Fig. 7 also indicates that PHE/PYR gain higher probability to stay in micelle core in mixed SDS-TX micelle (System III) than in pure SDS micelle (System I). Marqusee and Dill [61] proposed that most solutes, like arenes, should prefer the shell region of a spherical micelle due to the greater volume available there. By computing the micelle asymmetric parameter α defined by She et al. [62], it is interesting to find that α values for each system are around 0.10 meaning that the micelle is almost spherical in each simulation system. Hence, the entropic preference of PHE/PYR to occupy the larger volume of the micelle shell region may be one reason contributing to their preferable locus in micelle shell. Furthermore, though under cosolubilization conditions, PHE and PYR all prefer to stay in the shell, the movement of the two PAHs inside the micelle along with their different probability to contact with SDS heavy atoms (Fig. 4) indicates their different solubilization sites in the micelle, contributing to their possibility to coexist in the micelle.

Table 3
Percentage of simulation time for phenanthrene (PHE)/pyrene (PYR) to stay in micelle shell and core in the simulation system.[a]

Systems	Core (%)		Shell (%)	
	PHE	PYR	PHE	PYR
I	25 ± 3	21 ± 3	75 ± 3	79 ± 3
III	37 ± 8	33 ± 8	63 ± 8	67 ± 8

[a] When the COM distance between PAHs and micelle is within 1.2 nm means that PAHs are located in micelle core. When the COM distance is larger than 1.2 nm means that PAHs are in micelle shell. The total time used for analysis is 80 ns for System I and 120 ns for System III.

3.2.3. PAH-PAH interaction inside the micelle

The possibility of forming PAH dimers between two any PHE/PYR molecules in the micelle was examined, by computing the distance distribution between the COMs of PHE/PYR in Systems I and III. As shown in Fig. S8, the distance distribution between two PHEs, two PYRs, and mixed PHE-PYR obtains high probability in the range of 1.3–2.3 nm. However, within this distance range, it is found that SDS/TX molecules could intercalate between two PAH molecules [24]. Hence, to discard

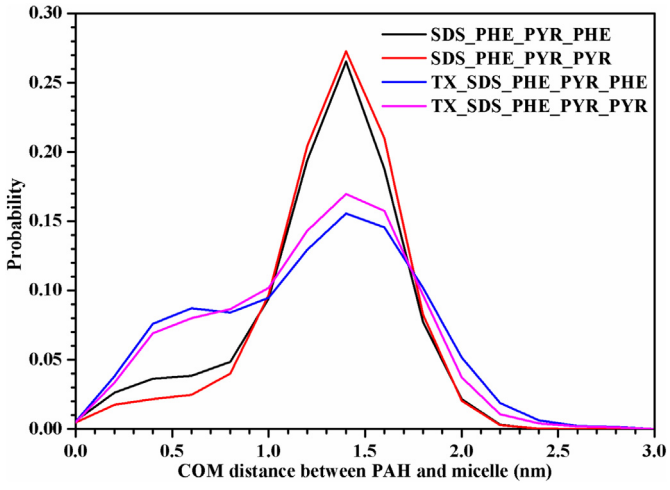

Fig. 7. Normalized probability distribution of the COM distance between PAH and micelle in Systems I and III. Black and red lines mean the probability for PHE and PYR observed in System I. Blue and magenta lines represent the probability for PHE and PYR obtained from System III.

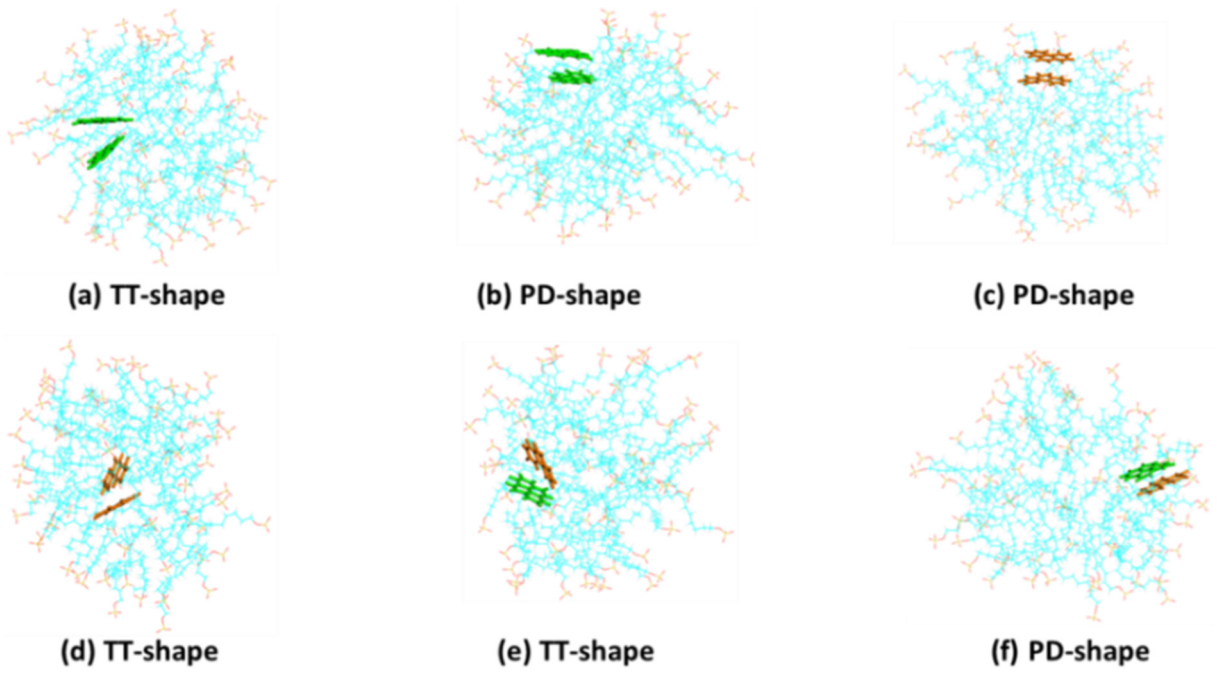

Fig. 8. (a–f) Examples showing the possible dimer configurations formed by pyrene (PYR, green), phenanthrene (PHE, orange) and mixed PHE-PYR extracted from System I.

this situation in the count of the numbers of dimers, a cutoff distance of 0.5 nm that used in Ref. [24] was selected to estimate the formation of dimer between two PHEs, two PYRs, and mixed PHE-PYR. Then the time percentage of PHE, PYR and mixed PHE-PYR to form dimer was computed by dividing the contacts when the COM distances between two PAH molecules are within 0.5 nm by their whole contacts. Results indicated that PHE, PYR and mixed PHE-PYR occupy 0.20%, 0.24% and 0.30% of the simulation time in System I and 0.20%, 0.29% and 0.19% of the simulation time in System III to form dimers.

PAH dimers can have various conformations (for instance parallel displaced (PD) and perpendicular (T-shaped, T) configurations). To examine this, the angle θ, defined as the angle between the normal vectors of the molecular planes of two PAH monomers, was computed. When θ equals to 0/180° or 90°, two PAH monomers form PD and T-shaped configurations, respectively. The other θ values correspond to the tilted T-shape (TT) configuration. Exemplified snapshots of dimer configurations formed by PHE, PYR, and PHE-PYR are shown in Fig. 8. Moreover, Figs. S9 and S10 depicted the distribution of dimer angle θ as a function of dimer distance. These figures show that the distribution of the θ values for PHE (0–80° and 100–180°) and mixed PHE-PYR (0–80° and 100–180°) is wider than that for PYR (0–40° and 140–180°), indicating that PHE, PYR and PHE-PYR could form PD and TT dimer configurations during the simulation time.

4. Conclusions

In this study, cosolubilization of PHE and PYR in single TX, SDS and mixed TX-SDS systems showed a synergistic solubilization effect. The synergistic extent decreased with increasing molar ratio of SDS in mixed micelle due to the decreasing micelle size. The presence of PHE and PYR in the shell and core regions of pure SDS and mixed SDS-TX micelle with a molar ratio of 1/1 was verified by computing the RDPs of PAH COM with respect to micelle COM from MD simulations. Cosolubilization of PHE and PYR could slightly change the internal structure of mixed SDS-TX micelle, yet no impact on pure SDS micelle. Though under cosolubilization conditions, both PHE and PYR prefer to stay in the shell, the different moving trajectories of the two PAHs in pure SDS and mixed SDS-TX micelle suggests that PHE and PYR have different solubilization sites to coexist in surfactant micelles.

Acknowledgement

XJ acknowledges the China Scholarship Council (No. 201406150028) and the CEA for the scholarship. This study was supported by the Science and Technology Planning Project of Guangdong Province (2014A020217002 and 2016B020242004), the Natural Science Foundation of China (No. 41330639), the China Postdoctoral Science Foundation (the 62nd grant No. 2908) and the granted access to the HPC resources of CCRT/CINES made by GENCI (Grand Equipement National de Calcul Intensif) under the allocations (t2015077426).

Appendix A. Supplementary data

Supplementary data to this article can be found online at https://doi.org/10.1016/j.molliq.2018.04.123.

References

[1] L.Y. Liu, J.Z. Wang, G.L. Wei, Y.F. Guan, C.S. Wong, E.Y. Zeng, Sediment records of polycyclic aromatic hydrocarbons (PAHs) in the continental shelf of China: implications for evolving anthropogenic impacts, Environ. Sci. Technol. 46 (2012) 6497–6504.
[2] Y. Zhang, S. Tao, Global atmospheric emission inventory of polycyclic aromatic hydrocarbons (PAHs) for 2004, Atmos. Environ. 43 (2009) 812–819.
[3] W. Xue, D. Warshawsky, Metabolic activation of polycyclic and heterocyclic aromatic hydrocarbons and DNA damage: a review, Toxicol. Appl. Pharmacol. 206 (2005) 73–93.
[4] O. Motorykin, M.M. Matzke, K.M. Waters, S.L. Massey Simonich, Association of carcinogenic polycyclic aromatic hydrocarbon emissions and smoking with lung cancer mortality rates on a global scale, Environ. Sci. Technol. 47 (2013) 3410–3416.
[5] M. Blumer, W.W. Youngblood, Polycyclic aromatic hydrocarbons in soils and recent sediments, Science 188 (1975) 53–55.
[6] X. Mao, R. Jiang, W. Xiao, J. Yu, Use of surfactants for the remediation of contaminated soils: a review, J. Hazard. Mater. 285 (2015) 419–435.
[7] C.N. Mulligan, R.N. Yong, B.F. Gibbs, Surfactant-enhanced remediation of contaminated soil: a review, Eng. Geol. 60 (2001) 371–380.
[8] A. Shah, S. Shahzad, A. Munir, M.N. Nadagouda, G.S. Khan, D.F. Shams, D.D. Dionysiou, U.A. Rana, Micelles as soil and water decontamination agents, Chem. Rev. 116 (2016) 6042–6074.

[9] H. Uchiyama, S.D. Christian, E.E. Tucker, J.F. Scamehorn, Solubilization of trichloroethylene by polyelectrolyte/surfactant complexes, AICHE J. 40 (1994) 1969–1975.
[10] J. Long, L. Li, Y. Jin, H. Sun, Y. Zheng, S. Tian, Synergistic solubilization of polycyclic aromatic hydrocarbons by mixed micelles composed of a photoresponsive surfactant and a conventional non-ionic surfactant, Sep. Purif. Technol. 160 (2016) 11–17.
[11] S. Li, Y. Pi, M. Bao, C. Zhang, D. Zhao, Y. Li, P. Sun, J. Lu, Effect of rhamnolipid biosurfactant on solubilization of polycyclic aromatic hydrocarbons, Mar. Pollut. Bull. 101 (2015) 219–225.
[12] J. Wei, G. Huang, H. Yu, C. An, Efficiency of single and mixed Gemini/conventional micelles on solubilization of phenanthrene, Chem. Eng. J. 168 (2011) 201–207.
[13] A.A. Dar, G.M. Rather, A.R. Das, Mixed micelle formation and solubilization behavior toward polycyclic aromatic hydrocarbons of binary and ternary cationic—nonionic surfactant mixtures, J. Phys. Chem. B 111 (2007) 3122–3132.
[14] M. Panda, D. Kabir ud, Solubilization of polycyclic aromatic hydrocarbons by gemini–conventional mixed surfactant systems, J. Mol. Liq. 187 (2013) 106–113.
[15] A. Srivastava, K. Ismail, Solubilization of polycyclic aromatic hydrocarbons in aqueous sodium dioctylsulfosuccinate solutions, J. Mol. Liq. 195 (2014) 105–109.
[16] L.A. Bernardez, S. Ghoshal, Selective solubilization of polycyclic aromatic hydrocarbons from multicomponent nonaqueous-phase liquids into nonionic surfactant micelles, Environ. Sci. Technol. 38 (2004) 5878–5887.
[17] X. Liang, M. Zhang, C. Guo, S. Abel, X. Yi, G. Lu, C. Yang, Z. Dang, Competitive solubilization of low-molecular-weight polycyclic aromatic hydrocarbons mixtures in single and binary surfactant micelles, Chem. Eng. J. 244 (2014) 522–530.
[18] J.D. Rouse, T. Morita, K. Furukawa, B.J. Shiau, Solubilization of mixed polycyclic aromatic hydrocarbon systems using an anionic surfactant, Colloids Surf. A Physicochem. Eng. Asp. 325 (2008) 180–185.
[19] X. Yang, G. Lu, B. She, X. Liang, R. Yin, C. Guo, X. Yi, Z. Dang, Cosolubilization of 4,4′-dibromodiphenyl ether, naphthalene and pyrene mixtures in various surfactant micelles, Chem. Eng. J. 260 (2015) 74–82.
[20] X. Yang, G. Lu, K. Huang, R. Wang, X. Duan, C. Yang, H. Yin, Z. Dang, Synergistic solubilization of low-brominated diphenyl ether mixtures in nonionic surfactant micelles, J. Mol. Liq. 223 (2016) 252–260.
[21] X. Yang, G. Lu, R. Wang, Y. Xie, C. Guo, X. Yi, Z. Dang, Competitive solubilization of 4,4′-dibromodiphenyl ether, naphthalene, and pyrene mixtures in Triton X series surfactant micelles: the effect of hydrophilic chains, Chem. Eng. J. 274 (2015) 84–93.
[22] P.A. Bhat, G.M. Rather, A.A. Dar, Effect of surfactant mixing on partitioning of model hydrophobic drug, naproxen, between aqueous and micellar phases, J. Phys. Chem. B 113 (2009) 997–1006.
[23] C. Honda, M. Itagaki, R. Takeda, K. Endo, Solubilization of pyrene in CnE_7 micelles, Langmuir 18 (2002) 1999–2003.
[24] X. Liang, M. Marchi, C. Guo, Z. Dang, S. Abel, Atomistic simulation of solubilization of polycyclic aromatic hydrocarbons in a sodium dodecyl sulfate micelle, Langmuir 32 (2016) 3645–3654.
[25] X.T. Wang, Y. Miao, Y. Zhang, Y.C. Li, M.H. Wu, G. Yu, Polycyclic aromatic hydrocarbons (PAHs) in urban soils of the megacity Shanghai: occurrence, source apportionment and potential human health risk, Sci. Total Environ. 447 (2013) 80–89.
[26] W. Zhang, C. Wei, C. Feng, Z. Yu, M. Ren, B. Yan, P. Peng, J. Fu, Distribution and health-risk of polycyclic aromatic hydrocarbons in soils at a coking plant, J. Environ. Monit. 13 (2011) 3429–3436.
[27] J.J. Deitsch, J.A. Smith, Effect of Triton X-100 on the rate of trichloroethene desorption from soil to water, Environ. Sci. Technol. 29 (1995) 1069–1080.
[28] W. Zhou, L. Zhu, Enhanced soil flushing of phenanthrene by anionic–nonionic mixed surfactant, Water Res. 42 (2008) 101–108.
[29] D. Mackay, W.Y. Shiu, K.C. Ma, S.C. Lee, Handbook of Physical-Chemical Properties. and Environmental Fate for Organic Chemicals, CRC press, 2006.
[30] C.H. Rycroft, G.S. Grest, J.W. Landry, M.Z. Bazant, Analysis of granular flow in a pebble-bed nuclear reactor, Phys. Rev. E 74 (2006), 021306.
[31] S. Abel, F.Y. Dupradeau, M. Marchi, Molecular dynamics simulations of a characteristic DPC micelle in water, J. Chem. Theory Comput. 8 (2012) 4610–4623.
[32] M. Shannigrahi, S. Bagchi, Novel fluorescent probe as aggregation predictor and micro-polarity reporter for micelles and mixed micelles, Spectrochim. Acta A 61 (2005) 2131–2138.
[33] R.G. Alargova, I.I. Kochijashky, M.L. Sierra, R. Zana, Micelle aggregation numbers of surfactants in aqueous solutions: a comparison between the results from steady-state and time-resolved fluorescence quenching, Langmuir 14 (1998) 5412–5418.
[34] X. Tang, K.J. Huston, R.G. Larson, Molecular dynamics simulations of structure–property relationships of Tween 80 surfactants in water and at interfaces, J. Phys. Chem. B 118 (2014) 12907–12918.
[35] H. Yan, P. Cui, C.B. Liu, S.-L. Yuan, Molecular dynamics simulation of pyrene solubilized in a sodium dodecyl sulfate micelle, Langmuir 28 (2012) 4931–4938.
[36] J.B. Klauda, R.M. Venable, J.A. Freites, J.W. O'Connor, D.J. Tobias, C. Mondragon-Ramirez, I. Vorobyov, A.D. MacKerell, R.W. Pastor, Update of the CHARMM all-atom additive force field for lipids: validation on six lipid yypes, J. Phys. Chem. B 114 (2010) 7830–7843.
[37] A.D. MacKerell, Molecular dynamics simulation analysis of a sodium dodecyl sulfate micelle in aqueous solution: decreased fluidity of the micelle hydrocarbon interior, J. Phys. Chem. 99 (1995) 1846–1855.
[38] D. Yordanova, I. Smirnova, S. Jakobtorweihen, Molecular modeling of Triton X micelles: force field parameters, self-assembly, and partition equilibria, J. Chem. Theory Comput. 11 (2015) 2329–2340.
[39] K. Vanommeslaeghe, E. Hatcher, C. Acharya, S. Kundu, S. Zhong, J. Shim, E. Darian, O. Guvench, P. Lopes, I. Vorobyov, A.D. Mackerell, CHARMM general force field: a force field for drug-like molecules compatible with the CHARMM all-atom additive biological force fields, J. Comput. Chem. 31 (2010) 671–690.
[40] X. Liang, C. Guo, Y. Wei, W. Lin, X. Yi, G. Lu, Z. Dang, Cosolubilization synergism occurrence in codesorption of PAH mixtures during surfactant-enhanced remediation of contaminated soil, Chemosphere 144 (2016) 583–590.
[41] H.J.C. Berendsen, D. van der Spoel, R. van Drunen, GROMACS: a message-passing parallel molecular dynamics implementation, Comput. Phys. Commun. 91 (1995) 43–56.
[42] D. Van Der Spoel, E. Lindahl, B. Hess, G. Groenhof, A.E. Mark, H.J.C. Berendsen, GROMACS: fast, flexible, and free, J. Comput. Chem. 26 (2005) 1701–1718.
[43] L. Martínez, R. Andrade, E.G. Birgin, J.M. Martínez, PACKMOL: a package for building initial configurations for molecular dynamics simulations, J. Comput. Chem. 30 (2009) 2157–2164.
[44] D.J. Price, C.L. Brooks, A modified TIP3P water potential for simulation with Ewald summation, J. Chem. Phys. 121 (2004) 10096–10103.
[45] G. Bussi, D. Donadio, M. Parrinello, Canonical sampling through velocity rescaling, J. Chem. Phys. 126 (2007), 014101.
[46] H.J.C. Berendsen, J.P.M. Postma, W.F. van Gunsteren, A. DiNola, J.R. Haak, Molecular dynamics with coupling to an external bath, J. Chem. Phys. 81 (1984) 3684–3690.
[47] M. Parrinello, A. Rahman, Polymorphic transitions in single crystals: a new molecular dynamics method, J. Appl. Phys. 52 (1981) 7182–7190.
[48] A. Rahman, F.H. Stillinger, Molecular dynamics study of liquid water, J. Chem. Phys. 55 (1971) 3336–3359.
[49] U. Essmann, L. Perera, M.L. Berkowitz, T. Darden, H. Lee, L.G. Pedersen, A smooth particle mesh Ewald method, J. Chem. Phys. 103 (1995) 8577–8593.
[50] C.D. Bruce, M.L. Berkowitz, L. Perera, M.D.E. Forbes, Molecular dynamics simulation of sodium dodecyl sulfate micelle in water: micellar structural characteristics and counterion distribution, J. Phys. Chem. B 106 (2002) 3788–3793.
[51] L. Zhu, S. Feng, Synergistic solubilization of polycyclic aromatic hydrocarbons by mixed anionic–nonionic surfactants, Chemosphere 53 (2003) 459–467.
[52] H. Siddiqui, M. Kamil, M. Panda, D. Kabir ud, Solubilization of phenanthrene and fluorene in equimolar binary mixtures of Gemini/conventional surfactants, Chin. J. Chem. Eng. 22 (2014) 1009–1015.
[53] W. Zhou, L. Zhu, Solubilization of pyrene by anionic–nonionic mixed surfactants, J. Hazard. Mater. 109 (2004) 213–220.
[54] S. Guha, P.R. Jaffé, C.A. Peters, Solubilization of PAH mixtures by a nonionic surfactant, Environ. Sci. Technol. 32 (1998) 930–935.
[55] S. Nagadome, Y. Okazaki, S. Lee, Y. Sasaki, G. Sugihara, Selective solubilization of sterols by bile salt micelles in water: a thermodynamic study, Langmuir 17 (2001) 4405–4412.
[56] R. Masrat, M. Maswal, A.A. Dar, Competitive solubilization of naphthalene and pyrene in various micellar systems, J. Hazard. Mater. 244–245 (2013) 662–670.
[57] T.Z. Wang, S.Z. Mao, X.J. Miao, S. Zhao, J.Y. Yu, Y.R. Du, ^{1}H NMR study of mixed micellization of sodium dodecyl sulfate and Triton X-100, J. Colloid Interface Sci. 241 (2001) 465–468.
[58] D.T. Allen, Y. Saaka, M.J. Lawrence, C.D. Lorenz, Atomistic description of the solubilisation of testosterone propionate in a sodium dodecyl sulfate micelle, J. Phys. Chem. B 118 (2014) 13192–13201.
[59] B. Aoun, V.K. Sharma, E. Pellegrini, S. Mitra, M. Johnson, R. Mukhopadhyay, Structure and dynamics of ionic micelles: MD simulation and neutron scattering study, J. Phys. Chem. B 119 (2015) 5079–5086.
[60] H. Cang, D.D. Brace, M.D. Fayer, Dynamic partitioning of an aromatic probe between the headgroup and core regions of cationic micelles, J. Phys. Chem. B 105 (2001) 10007–10015.
[61] J.A. Marqusee, K.A. Dill, Solute partitioning into chain molecule interphases: monolayers, bilayer membranes, and micelles, J. Chem. Phys. 85 (1986) 434–444.
[62] A.Q. She, H.Z. Gang, B.Z. Mu, Temperature influence on the structure and interfacial properties of surfactin micelle: a molecular dynamics simulation study, J. Phys. Chem. B 116 (2012) 12735–12743.